# Enhanced adhesion of mildly positively charged vesicles to endothelial cells with shed glycocalyx

**Manuel M. Sirch, David Wörle, Marina G. Huber, Christoph Westerhausen**

**Angaben zur Veröffentlichung / Publication details:**

Sirch, Manuel M., David Wörle, Marina G. Huber, and Christoph Westerhausen. 2025. "Enhanced adhesion of mildly positively charged vesicles to endothelial cells with shed glycocalyx." *ACS Omega* 10 (15): 14858–65. https://doi.org/10.1021/acsomega.4c10054.

ACS OMEGA

Open Access



http://pubs.acs.org/journal/acsodf

Article

# Enhanced Adhesion of Mildly Positively Charged Vesicles to Endothelial Cells with Shed Glycocalyx

Manuel M. Sirch, David Wörle, Marina G. Huber, and Christoph Westerhausen*

Cite This: *ACS Omega* 2025, 10, 14858−14865

Read Online

ACCESS | Metrics & More | Article Recommendations | Supporting Information

**ABSTRACT:** The glycocalyx of endothelial cells is a dynamic, gel-like layer of glycoproteins, proteoglycans, and glycolipids that lines the luminal surface of blood vessels, playing a critical role in vascular permeability, mechanotransduction, and protection against shear stress. In this study, we investigated the in vitro adhesion of giant unilamellar vesicles (GUVs) composed of 1,2-dioleoyl-3-trimethylammonium-propane (DOTAP) and 1,2-dimyristoyl-*sn*-glycero-3-phosphocholine (DMPC). Specifically, we examined mildly positively charged DOTAP-DMPC (20:80) GUVs, based on positively charged DOTAP and neutral DMPC but exhibiting an overall mild positive charge in physiological buffer, and neutral DMPC GUVs, which show a negative charge in physiological buffer. Adhesion to human umbilical vein endothelial cells (HUVEC) was studied under three culture conditions: dynamic (intact glycocalyx), static (underdeveloped glycocalyx), and glycocalyx-shed (degraded glycocalyx). Vesicles were produced via electroformation, stained with Texas Red dye, and perfused over endothelial cells at a controlled velocity to simulate slow blood flow. Adhesion was tracked using fluorescence microscopy combined with cell segmentation techniques. Adhesion of DOTAP-DMPC vesicles was significantly enhanced—by approximately 3.5-fold—on glycocalyx-shed cells compared to cells with an intact glycocalyx. In contrast, DMPC vesicles showed no adhesion under any condition. Analysis of vesicle size distributions revealed no significant differences between adherent and nonadherent vesicles or between DOTAP-DMPC and DMPC vesicles. These findings provide insights into the role of the endothelial glycocalyx in regulating adhesion, with potential implications for tumor cell interactions with the endothelium and mechanisms underlying DOTAP-based transfection.

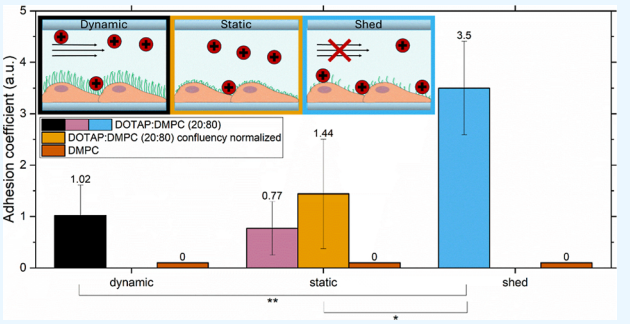




## INTRODUCTION

Cationic 1,2-dioleoyl-3-trimethylammonium-propane (DOTAP) vesicles are commonly used in transfection to facilitate the delivery of genetic material into cells. These vesicles form lipoplexes by encapsulating DNA or RNA, allowing the genetic material to cross cell membranes efficiently.[1,2] The positive charge of DOTAP vesicles interacts with the negatively charged nucleic acids, creating a stable complex that can be endocytosed by target cells. This method is widely used in gene therapy research, vaccine development, and molecular biology studies due to its effectiveness in delivering nucleic acids into a wide variety of cell types.[3−5]

For endocytic uptake or fusion, DOTAP vesicles must first adhere to the cell membrane to deliver their genetic cargo. However, for endothelial cells subjected to physiological conditions, particularly the application of shear stress, the presence of the endothelial glycocalyx and changes of the membrane properties significantly alter this interaction.[6−10]

The endothelial glycocalyx is a highly specialized, carbohydrate-rich layer that coats the surface of endothelial cells. It consists mainly of proteoglycans, glycosaminoglycans (GAGs), and glycoproteins.[11] Proteoglycans, such as syndecans and glypicans, anchor the glycocalyx to the cell membrane, while GAGs like heparan sulfate contribute to its negative charge, which is key to many of its functions.[12] This negative charge helps create an electrostatic barrier that influences how molecules interact with the cell surface, attracting water and ions while repelling or controlling the movement of other molecules.[13,14] The glycocalyx regulates vascular permeability, acting as a selective barrier for solutes and proteins, and plays a key role in preventing unwanted adhesion of blood cells and platelets. Additionally, it is essential in mechanotransduction, as it senses and transmits shear stress signals from blood flow to the underlying endothelial cells.[15]

The glycocalyx is formed and maintained when endothelial cells are exposed to shear stress for a specific duration, which is typically several hours to days.[16] When shear stress is absent or significantly reduced, endothelial cells begin to shed or degrade

**Received:** November 4, 2024
**Revised:** January 15, 2025
**Accepted:** January 22, 2025
**Published:** April 10, 2025

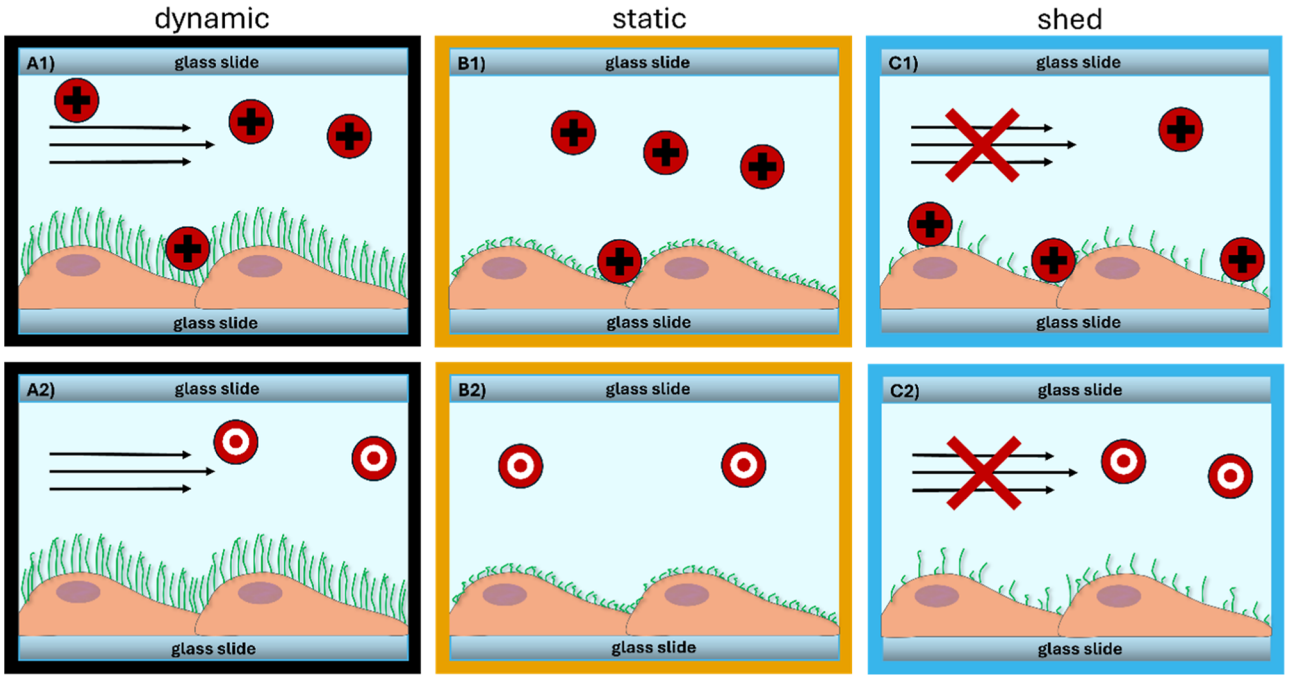


**Figure 1.** Schematic illustration of culture conditions and adhesion of mildly positively charged DOTAP-DMPC GUVs and DMPC GUVs. (A) Dynamically cultured HUVEC with a well-developed glycocalyx are exposed to GUVs (B) statically cultured HUVEC with an underdeveloped glycocalyx are exposed to GUVs. (C) Dynamically cultured HUVEC which shed the glycocalyx due to flow interruption are exposed to GUVs.

their glycocalyx within a few hours, leading to a vulnerable exposure of the endothelium.[17−19] This shear stress not only influences the glycocalyx but also plays a significant role in altering the physical properties of the endothelial cell membrane, particularly its fluidity. Under sustained shear stress, the cell membrane becomes more fluid, allowing for greater flexibility and adaptability in response to mechanical forces.[20,21] Shear stress can also affect the lipid composition of the membrane, further promoting a transition from a more ordered, gel-like phase to a more disordered, fluid phase.[22] This shift enhances the lateral mobility of lipids and membrane proteins, facilitating processes such as adhesion properties and therefore also have a direct effect on endocytosis and vesicle fusion.[23−25]

In this study, we investigate how shear stress and the presence of the glycocalyx impact the adhesion of DOTAP-DMPC (20:80) giant unilamellar vesicles (GUVs), which show a mild positive charge in Dulbecco's phosphate-buffered saline (DPBS) and normally uncharged 1,2-dimyristoyl-*sn*-glycero-3-phosphatidylcholine (DMPC) GUVs, which show a negative charge in the buffer, to in vitro cultured human umbilical vein endothelial cells (HUVEC). To explore this, we compare vesicle adhesion under three distinct culture conditions: (1) cells cultured under dynamic conditions that maintain an intact glycocalyx Figure 1A, (2) cells cultured under static conditions, where the glycocalyx is underdeveloped Figure 1B, and (3) cells cultured dynamically but incubated without shear flow, resulting in glycocalyx shedding before the adhesion experiments Figure 1C. These conditions allow us to evaluate how the presence or absence of the glycocalyx, along with changes in membrane dynamics, influence the interaction between the vesicles and the endothelial cells.

Our results show that adhesion to glycocalyx-shed cells increased by approximately 3.5 times compared to both statically and dynamically cultured cells with an intact glycocalyx, which exhibited no significant differences in adhesion. In contrast, no adhesion was observed when using pure DMPC vesicles in the same experiment.

## MATERIALS AND METHODS

**Cell Culture and In Vitro Dynamic Conditions.** Commercially available HUVEC (product number PB-CH-190-8013), pooled from multiple donors and obtained from PELOBIOTECH (Planegg, Germany), were used along with endothelial cell culture medium (Product number PB-MH-100-2100) from the same supplier. The cells were maintained at 37 °C in a humidified atmosphere with 5% $CO_2$ and were used between passages 2 and 5. For each experimental condition—dynamic conditions with an intact glycocalyx, static conditions without a well-developed glycocalyx, and dynamic conditions with a shed glycocalyx—cells from the same passage and batch were used to ensure consistency. Different batches of pooled cells were used for each set of experiments.

Cells were seeded at the manufacturer recommended concentrations of $2 \times 10^5$ cells/ml for static conditions and $1 \times 10^6$ cells/ml for dynamic conditions in ibidi (Martinsried, Germany) polymer-bottom channel slides (height: 800 $\mu$m, product number 80196) coated with rat tail collagen type I (product number CLS354236) from Cornig (New York, United States). HUVEC under dynamic and shed conditions were cultured for 6 days under a constant, unidirectional shear stress of 6 dyn/cm$^2$ using an ibidi pump system. For the shed condition, cells were disconnected from the pump 2 h prior to the experiment to allow for glycocalyx degradation. Cells under static conditions were seeded 6 days prior to the experiment and were not exposed to shear stress. The cell culture medium was changed every 2 days, and to prevent glycocalyx degradation during dynamic conditions, the pump system


https://doi.org/10.1021/acsomega.4c10054
ACS Omega 2025, 10, 14858−14865

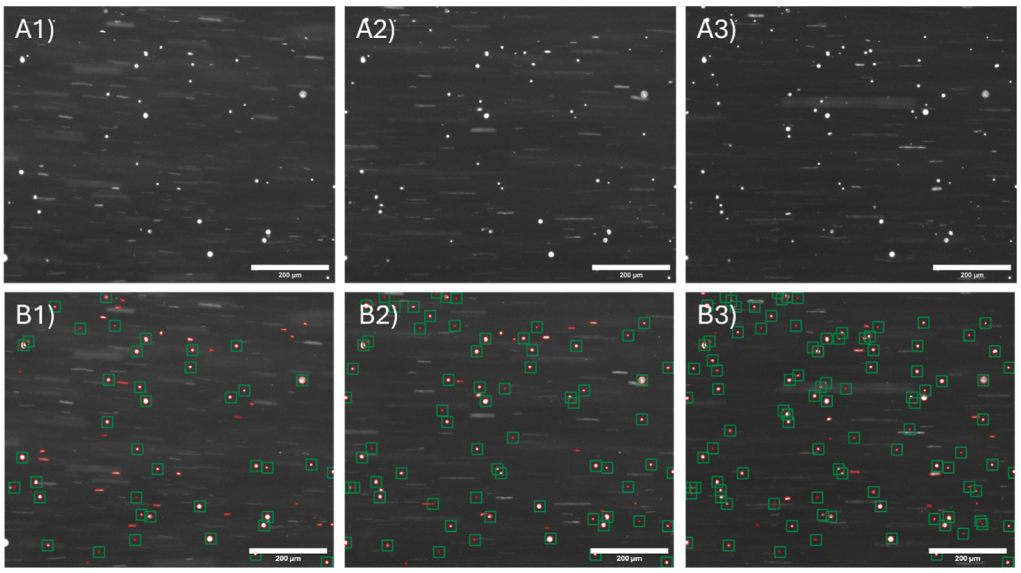


**Figure 2.** Exemplary fluorescence image analysis of vesicles adhering to the surface. (A1−A3) Grayscale images captured at 30, 90, and 150 s, showing fluorescent signals from Texas Red-stained vesicles. (B1) Vesicle detection using Cellpose 2.0, with red circles indicating vesicles identified in the focal plane. (B2) Adherent vesicles, those that remained stationary, are marked by green squares. (B3) Increasing number of adherent vesicles over time.

was positioned next to a sterile bench to enable rapid medium changes within approximately 30 s.

The integrity of the glycocalyx under dynamic conditions was verified using staining with commercially available Alexa Fluor 555 conjugated wheat germ agglutinin (WGA) (product number W32464) also purchased from Thermo Fisher, as described in the Supporting Information section. This method ensured accurate assessment of glycocalyx presence and condition across experimental setups. We observed a significant difference in Alexa Fluor 555 staining intensity among the three culture conditions. Dynamically cultured cells exhibited an intensity more than four times higher than that of statically cultured cells and more than twice as high as cells under shedding conditions.

**Adhesion Measurement of GUVs on the Cell Surface.** Positively and neutrally charged GUVs, stained with Texas Red dye, were generated via electroformation and used to assess their adhesion to the cell surface, depending on the presence of an intact glycocalyx and the cultivation method. Imaging was performed using a ZEISS Axio Observer 7 microscope equipped with a 10× magnification objective.

**Preparation of the GUVs.** An incubation chamber with a volume of 6.2 mL made of two zinc-oxide coated glass slides and a Teflon spacer with a thickness of 5 mm and two holes was used to produce the GUVs. The glass slides and spacer were first cleaned in isopropyl alcohol using an ultrasonic bath for 30 min, rinsed with ultrapure water, and dried with nitrogen airflow. DMPC (product number 850345) and DOTAP (product number 890890) lipids purchased from Avanti Polar Lipids (Alabaster, Alabama, United States) were diluted in chloroform to a concentration of 10 mg/mL (DMPC and 20:80 DOTAP-DMPC mix), with 5% Texas Red DHPE (product number T1395MP) bought from Thermo Fisher (Waltham, Massachusetts, United States), added for fluorescence. After mixing, 50 $\mu$L of the lipid solution was applied to the uncoated surface of one slide, and the other slide was placed on top. The slides were pulled apart to create a thin lipid film and dried in a vacuum desiccator for 10 min. The Teflon spacer was then positioned between the slides, which were clamped together, and a sucrose (Sigma-Aldrich Chemie GmbH, Taufkirchen, Germany, product number 1076871000) solution, adjusted to 0.01 M was injected to fill the chamber. The chamber was placed in a heat bath with a temperature 10 °C above the phase transition temperature of DMPC (24.1 °C) and a frequency generator was connected to apply a 1 V square wave signal at 10 Hz for 15 min, followed by the same signal with an increased amplitude of 4 V for 2 h. Afterward, the vesicle suspension was collected and stored the dark in an aluminum foil-wrapped vial protected from light to prevent bleaching at 8 °C, where it could be kept for several weeks.

**Experimental Setup.** A funnel used as a reservoir was screwed into one side of the channel slides. The opposite side was connected to a 1.6 mm inner diameter tube, which was attached to another syringe placed in a syringe pump. A flow rate of 20 $\mu$L/min, corresponding to a flow velocity of 5 mm/min in the channel, was set with the pump operating in reverse mode to draw fluid into the syringe. Experiments were conducted consistently in the center of the channel slide, where, according to ibidi (application note 3), the shear stress is uniform at approximately $\tau \approx 0.70$ dyn/cm$^2$ within the area captured by the microscope. The stage incubator was preheated to 37 °C, and the microscope objective was positioned at the center of the channel, capturing an image of the cells in phase contrast. The vesicle solution was diluted 1:25 with 1x DPBS (Product number D8537-6X500ML) from Sigma-Aldrich and introduced into the reservoir. The vesicle solution was manually pumped into the channel until it reached the area under the microscope objective. The focus was then adjusted to ensure the vesicles on the cell surfaces were clearly visible, and a reference image was captured to identify the initial number of vesicles $N_0$. Once the pump was started, images were taken every 30 s, continuing until a total of 25 images had been recorded.

**Image Analysis.** To ensure accurate measurement of GUVs adhering to the cell surface rather than the bottom of the channel slide, a phase-contrast image of the cell layer was


https://doi.org/10.1021/acsomega.4c10054
ACS Omega 2025, 10, 14858−14865

captured before the experiment. This image was then segmented using the Cellpose 2.0 algorithm,[26] as illustrated in Figure 4 A1 and A2.

Cellpose 2.0 was also used to analyze lipid vesicle adhesion by tracking the number of vesicles on a cell layer throughout measurements by identifying masks and diameters in images, counting detectable adherent vesicles as well as cells, assessing cell confluence.

As demonstrated in Figure 2 the customized script creates objects with attributes like position and radius from individual masks, where position is the mean of pixel positions, and radius assumes a circular shape. These objects help compare positions to track vesicle adhesion. By comparing vesicle positions in consecutive images within a tolerance radius, the script identifies whether a vesicle adheres to the surface. Adherent vesicles, detected over a specified period, are subclassed and characterized by attributes like the detection time and consistency across images. The complete script is available at https://github.com/DavidWoerle/celladhesion for reproducibility.

**Confocal Microscopy.** A Stellaris 5 confocal microscope with 63× magnification was used to obtain additional detailed data on the position and morphology of the vesicles. The membrane of cells in channel slides where vesicle adhesion had already been measured was stained with Laurdan for this purpose.

Laurdan bought from Sigma-Aldrich (product number 40227) was diluted to 5 mg/mL in chloroform and then exposed to a continuous flow of nitrogen for 30 min to evaporate the chloroform. After that, 500 $\mu$L of DMSO (product number 4-X) purchased from ATCC (Manassas, Virginia, United States) was added and placed in an ultrasonic bath for 30 min at a temperature of 50 °C. The Laurdan solution was finally mixed with 50 mL HUVEC cell culture medium.

The staining process involved replacing the cell culture medium in the pump system with Laurdan solution. For statically cultured cells, this required connecting them to the pump system, while shed cells were stained after stopping the flow. Flow was resumed to allow dye incubation for 2 h. Afterward, the channel slide was rinsed sequentially with 2 mL of DPBS and 2 mL of medium to remove excess dye and prepare the cells for imaging.

Laurdan-stained cells were illuminated with a 405 nm laser, while a white light laser at 569 nm was used to excite the Texas Red-labeled vesicles. The channel slides were mounted on the microscope stage, and cells were first located with a 20× magnification. The bottom of the slides was then identified precisely using the 63× magnification. A z-scan was conducted, capturing images at 0.5 $\mu$m intervals from the bottom of the slide upward until no more cells or vesicles were visible.

**Cytometer Measurements for Vesicle Size Comparison.** A Beckman Coulter CytoFlex (Brea, California, United States) cytometer was utilized to measure the Forward Scattering Area (FSC-A) of the giant unilamellar vesicles (GUVs) used in the experiment. For this analysis, 100 $\mu$L of vesicle solution was introduced into the cytometer, which operated at a flow rate of 30 $\mu$L/min.

**Zeta Potential Measurement.** To assess the surface charge characteristics of the GUVs in the used experimental solution, a Zetasizer Ultra (Malvern Panalytical, Worcestershire, United Kingdom) was utilized to measure the zeta potential at 37 °C. Three runs for each DMPC and DOTAP-DMPC GUVs were performed.

## RESULTS

To establish a metric for quantifying the adhered vesicles the total number of adherent GUVs $N_{adh}$ per image, as well as the overall count $N_0$ of detected objects on the first image without active perfusion are counted. A normalization method accounts for vesicle concentration, yielding an adhesion quotient

$$A = \frac{N_{adh}}{N_0}$$

as a measure of GUV adhesion. The confluence of the cell layer is critical, with only vesicles adhering to the cell lawn considered relevant.

Figure 3 shows the contrasting adhesion behaviors of pure DMPC vesicles and 20:80 DOTAP-DMPC vesicles on the HUVEC layer under different culturing conditions. To account for the potential reduction in adhesion area in statically cultured cells, as seen in the segmentation of Figure 4A, additionally the adhesion coefficient was normalized by dividing it by the percentage of confluency (yellow column in Figure 3).

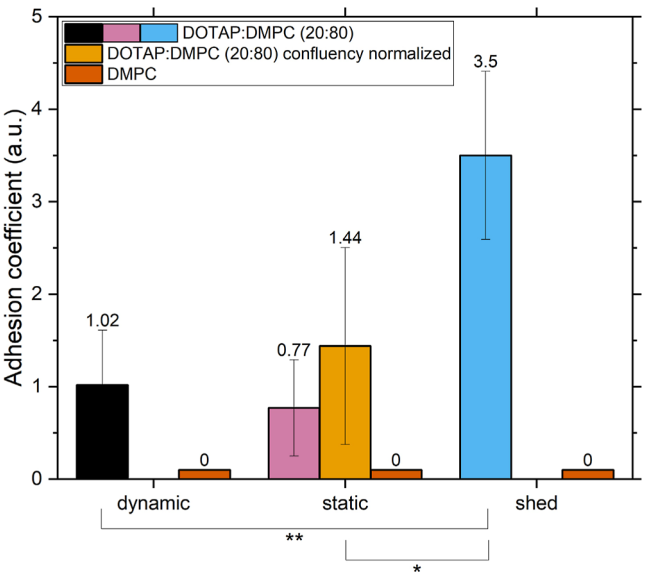


**Figure 3.** Adhesion coefficients of GUVs adhering to the cell surface. HUVEC under the shedding condition show significant increase of mildly positively charged DOTAP-DMPC (20:80) GUV adhesion in comparison to dynamic and static culture conditions. Cells under dynamic and static culture conditions show no significant difference between each other. No adhesion could be measured for pure DMPC GUVs, regardless of the culture method. The sample size of analyzed slides was $N = 6$ for dynamically cultured cells, $N = 6$ for statically cultured cells and $N = 4$ for cells under the shedding condition. **: $p < 0.01$, *:$p < 0.05$.

For DMPC vesicles, no adhesion was observed across all conditions (static, dynamic, or shed), highlighting their inert interaction with the endothelial layer.

In contrast, the 20:80 DOTAP-DMPC vesicles displayed more complex adhesion dynamics. Adhesion coefficients for both statically and dynamically cultured cells ranged from 0.77 to 1.44, with no significant difference, even after the normalization for the confluency differences. However, under



https://doi.org/10.1021/acsomega.4c10054
ACS Omega 2025, 10, 14858−14865

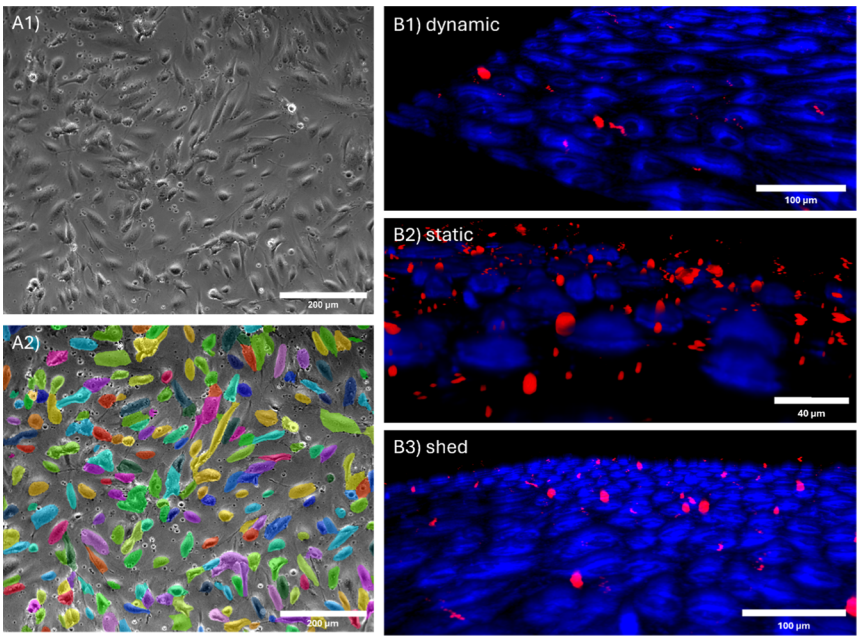


**Figure 4.** Cell Layer Segmentation and GUV Positions. (A1) Phase-contrast microscopy of a statically cultured HUVEC layer before GUV perfusion reveals loosely spaced cells lacking the cobblestone morphology typical of dynamic cultures. (A2) A segmented cell mask of the HUVEC layer generated with Cellpose 2.0, showing significant intercellular spaces. Vesicles adhering outside these colored regions are excluded from adherence counts in subsequent analyses. (B1) Confocal microscopy of a dynamically cultured HUVEC sample after GUV perfusion, with cell membranes in blue and GUVs in red. The confluent cell layer demonstrates minimal vesicle adherence to cell surfaces. (B2) Confocal microscopy of statically cultured HUVEC showing wider intercellular gaps, with numerous vesicles adhering in these spaces; however, these vesicles are excluded from adherence counts as they are not directly bound to cell surfaces. (B3) Confocal microscopy of dynamically cultured HUVEC under glycocalyx-shed conditions shows a highly confluent cell layer where GUVs adhere directly to cell surfaces, indicating enhanced binding.

**Table 1. Summary of the Performed Statistical Analysis for the Adhesion Coefficients**

| descriptive statistics | | | | Shapiro–Wilk test | one-way ANOVA with Tukey comparisons | |
|---|---|---|---|---|---|---|
| category | mean | standard deviation | N (slides) | passed normality test | comparison | adjusted *p*-value |
| static | 1.4388 | 1.0648 | 6 | yes | static vs dynamic | 0.7138 ns |
| dynamic | 1.0167 | 0.6455 | 6 | yes | static vs shed | 0.01110 * |
| shed | 3.495 | 1.0497 | 4 | yes | dynamic vs shed | 0.002974 ** |

shedding conditions, adhesion increased significantly, with an average coefficient of 3.5, indicating a much stronger attachment to the cell layer.

Statistical analyses (Table 1) included a Shapiro–Wilk test to confirm the normality of the data and a one-way ANOVA followed by Tukey's multiple comparison test to assess group differences.

Analysis of the confocal data as exemplary shown in Figure 4B revealed that the cells were found to cluster at cell–cell junctions, indicating that these contact points may play a role in vesicle adhesion under varying culture conditions. Notably, a significant portion of the vesicles were adhering to the bottom of the slide, often located between cells rather than directly on their surfaces. These vesicles were appropriately excluded from the count of surface-adhered vesicles.

To address potential contributions of size differences between the different kinds of GUVs two size determinations have been applied: a micrograph-based one and additionally a comparison using a cytometer. The data is shown in Figure 5. The analysis of vesicle size distributions in Figure 5A highlights trends between nonadherent and adherent GUVs, as well as between DOTAP-DMPC and pure DMPC GUVs.

Nonadherent GUVs exhibit a mean diameter of 9.47 $\mu$m ($\pm$4.42 $\mu$m) and a median of 8.78 $\mu$m, based on a total of 12,484 vesicles. Adherent GUVs, in contrast, display a smaller mean diameter of 7.10 ($\pm$3.78 $\mu$m) and a median of 6.21 $\mu$m, derived from 1876 vesicles.

Similarly, the comparison between DOTAP-DMPC and pure DMPC GUVs reveals a difference in size. DOTAP-DMPC GUVs show a mean diameter of 9.16 ($\pm$4.43 $\mu$m) and a median of 8.28 $\mu$m from 14,362 vesicles. Pure DMPC GUVs, meanwhile, exhibit a larger mean diameter of 10.61 ($\pm$5.39 $\mu$m) with a median of 8.97 $\mu$m, though this measurement is based on only 381 vesicles. The limited sample size for pure DMPC GUVs reflects observations made immediately after the sedimentation phase, as no vesicles could be identified as adherent or temporarily adherent beyond this point.

The comparison of cytometer measurements between DOTAP-DMPC GUVs and DMPC GUVs in Figure 5B shows a visible overlap in size distribution, but it is clearly evident that the DMPC vesicles exhibit a broader distribution, indicating a larger range of vesicle sizes. For each sample, data from 10,000 vesicles were recorded, with event rates of 41 events/s for the DOTAP-DMPC sample and 54 events/s for the DMPC sample. This higher event rate for DMPC suggests a slightly higher concentration of vesicles in the sample.

The overlap, broader distribution, and higher vesicle concentration observed in the DMPC sample suggest that



https://doi.org/10.1021/acsomega.4c10054
ACS Omega 2025, 10, 14858–14865

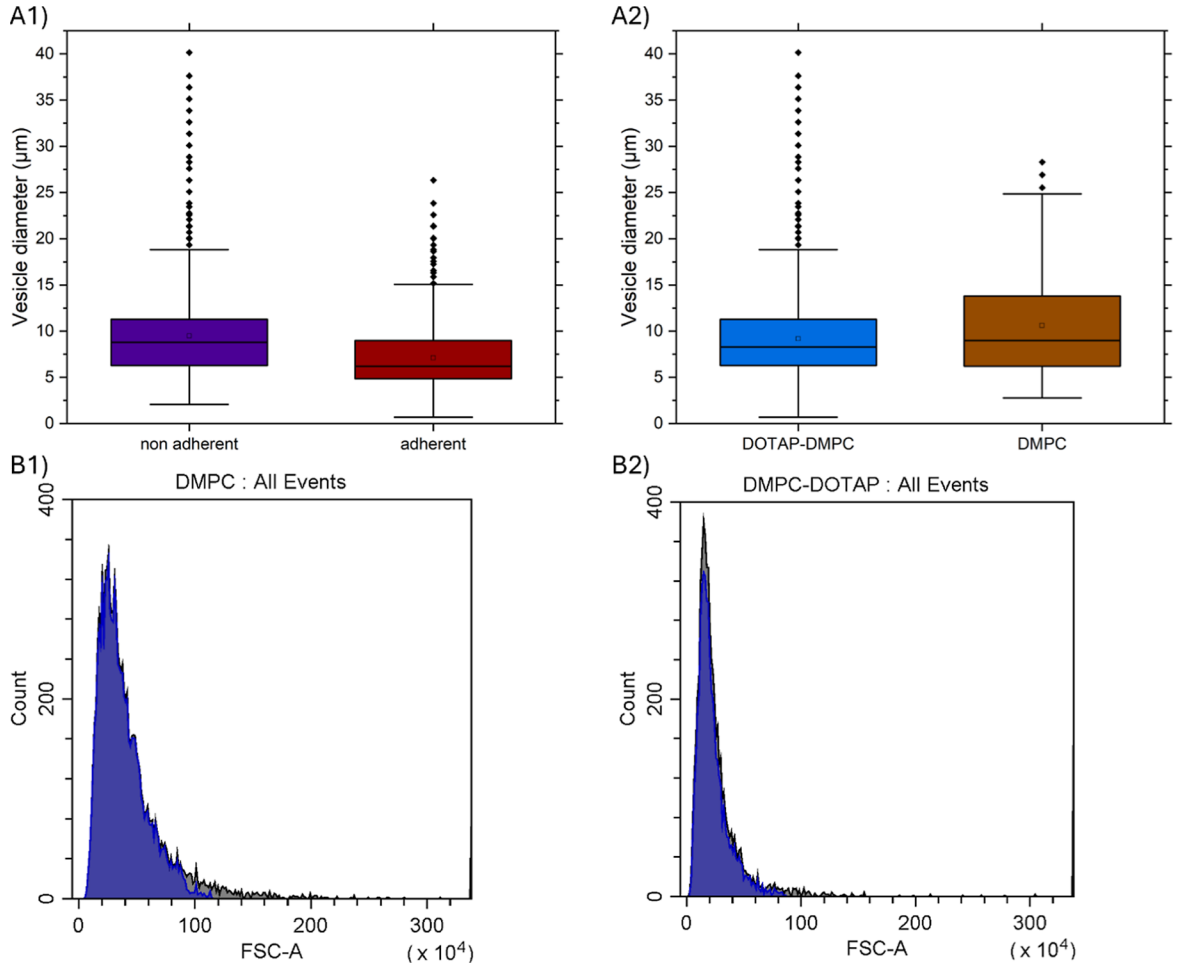


**Figure 5.** Boxplots and Histograms of Size Distribution of GUVs. (A1) Comparison of size distributions between nonadherent and adherent GUVs for all recorded DOTAP-DMPC vesicles. The mean diameter of nonadherent GUVs is 9.47 ± 4.42 $\mu$m, with a median diameter of 8.78 $\mu$m ($N$ = 12,484 vesicles). For adherent GUVs, the mean diameter is 7.10 ± 3.78 $\mu$m and the median is 6.21 $\mu$m ($N$ = 1876 vesicles). (A2) Comparison of size distributions between DOTAP-DMPC GUVs and pure DMPC GUVs. The mean diameter of DOTAP-DMPC GUVs is 9.16 ± 4.43 $\mu$m, with a median of 8.28 $\mu$m ($N$ = 14,362 vesicles). In contrast, pure DMPC GUVs have a mean diameter of 10.61 ± 5.39 $\mu$m and a median of 8.97 $\mu$m ($N$ = 381 vesicles). The dots above the whiskers represent the outliers. (B1) FSC-A of the DOTAP-DMPC GUVs, (B2) FSC-A of the DMPC GUVs. The vesicle count for each measurement was $N$ = 10,000. A higher FSC-A correlates with larger vesicles. The blue graph represents P1 (primary gate to isolate the main cell population, excluding debris and doublets), gray represents all events.

there are sufficient GUVs of the same size as the adhering DOTAP-DMPC vesicles present within the DMPC population, as discussed below.

To quantify the difference in surface charge zeta potentials of the GUVs have been measured. The DMPC GUVs exhibited a zeta potential of −7.41 ± 0.24 mV, reflecting a negatively charged surface under the experimental conditions. In contrast, the DOTAP-DMPC GUVs displayed a zeta potential of +2.29 ± 0.17 mV, showing a shift toward an overall positively charged surface due to the incorporation of DOTAP.

## DISCUSSION

The Zeta potential measurements of DMPC GUVs reveal that their surface charge becomes more negative when suspended in an ionic buffer medium like DPBS and maintained above their phase transition temperature, as Morini et al. reported earlier. This behavior indicates that pure DMPC vesicles, although zwitterionic in composition, are not entirely neutral under these conditions. The increased negative charge can exacerbate electrostatic repulsion between the DMPC vesicles and the negatively charged glycocalyx and cell membrane, preventing effective adhesion.[27]

The addition of positively charged DOTAP lipids, which leads to the overall positive charge of the GUVs, introduces electrostatic interactions between the vesicles and the negatively charged cell membrane and glycocalyx, enabling 20:80 DOTAP-DMPC vesicles to adhere under both static and dynamic conditions, as reflected by the observed adhesion coefficients.[28,29]

During glycocalyx shedding, proteolytic enzymes cleave glycoproteins and proteoglycans, producing negatively charged fragments that can interact with the positively charged vesicle surface, enhancing adhesion. Shedding not only disrupts protein−protein interactions within the glycocalyx but also releases proteins that could promote vesicle adhesion through interactions with surface proteins or receptors.[28,30,31] Furthermore, shedding exposes membrane-associated proteins or glycolipids with membrane-spanning domains or lipid anchors, which may provide additional binding sites for vesicles.[28,30−32] Membrane-bound proteins, such as integrins, cadherins, and others, enable specific molecular interactions beyond simple


https://doi.org/10.1021/acsomega.4c10054
ACS Omega 2025, 10, 14858−14865

electrostatics, including receptor−ligand binding and interactions mediated by membrane-associated proteins, which are crucial for adhesion under both static and dynamic conditions.[33,34]

Shedding exposes these surface proteins that normally lie beneath the glycocalyx, which can further facilitate vesicle adhesion. This may explain why vesicles adhere more effectively even when the glycocalyx is present in a modified or reduced state. Thus, the ability of the cell membrane to provide multiple interaction points beyond just charge-based adhesion suggests that it plays a more influential role in vesicle adhesion than the glycocalyx alone.[35,36]

In addition to the presence of these proteins, the lipid composition and organization of the cell membrane, including the formation of lipid rafts—possibly due to the cultivation under shear stress—can also contribute to adhesion. Lipid rafts, which are microdomains rich in cholesterol and sphingolipids, may act as preferential docking sites for vesicles due to their ability to concentrate adhesion-related proteins. These membrane regions could serve as key platforms for vesicle interaction, allowing for strong adhesion independent of the glycocalyx.[37,38]

Another important aspect to consider is the vesicle diameter. The size distributions of adherent and nonadherent GUVs, as well as those of the DMPC and DOTAP-DMPC GUVs, show significant overlap. This indicates that the observed differences cannot predominantly be driven by size variations. The vesicle sizes in this study also align with the typical diameters of circulating tumor cells (CTCs), which range between 8 and 20 $\mu$m.[39] This similarity is particularly relevant because it suggests that the mechanisms governing vesicle adhesion to endothelial cells may also provide insight into how CTCs interact with the endothelium during metastasis.

## CONCLUSION

This study highlights the pivotal role of the endothelial glycocalyx in regulating vesicle adhesion, as evidenced by the distinct behavior of vesicles: negatively charged DMPC vesicles in DPBS, despite being composed of lipids that are supposed to be neutrally charged, and mildly positively charged DOTAP-DMPC (20:80) vesicles, formed from a combination of positively charged DOTAP and DMPC. The negatively charged glycocalyx of HUVEC repels the negatively charged DMPC vesicles, preventing adhesion under both static and dynamic conditions. However, incorporating positively charged DOTAP lipids enables vesicle adhesion by introducing electrostatic interactions with the cell membrane. Notably, vesicle adhesion significantly increases when the glycocalyx is shed, possibly exposing additional binding sites and membrane-associated proteins that further enhance vesicle attachment.

The findings highlight that vesicle surface charge, as well as the condition of the endothelial glycocalyx, are critical factors in determining vesicle adhesion to the endothelium. Furthermore, the observed size of these vesicles aligns with known size distributions of circulating tumor cells, offering potential insights into the processes of early metastatic adhesion. Further exploration into glycocalyx modulation and its impact on cell adhesion properties could advance the understanding of vesicle and cell interactions with the endothelium, with possible implications for drug delivery, vascular health, and metastasis.

## ASSOCIATED CONTENT

### Data Availability Statement

The data sets used and/or analyzed during the current study are available at https://github.com/DavidWoerle/celladhesion-data. However, the raw data supporting Figure S1 (WGA staining of the glycocalyx) is not publicly available as it is currently under review for another manuscript. This data can be made available upon reasonable request once the review process is complete.

### Supporting Information

The Supporting Information is available free of charge at https://pubs.acs.org/doi/10.1021/acsomega.4c10054.

Verification of intact glycocalyx under dynamic culture conditions using fluorescence staining with Alexa Fluor 555-conjugated wheat germ agglutinin (WGA); statistical analysis of glycocalyx fluorescence intensities under dynamic, static, and shedding conditions; mean fluorescence values; ANOVA results; Supplementary Figure S1: exemplary fluorescence images of HUVEC under dynamic, static, and shedding conditions (PDF)

## AUTHOR INFORMATION


### Corresponding Author

**Christoph Westerhausen** − *Institute of Theoretical Medicine, Physiology, University of Augsburg, Augsburg 86159, Germany; Institute of Physics, University of Augsburg, Augsburg 86159, Germany; Center for NanoScience (CeNS), Ludwig-Maximilians-Universität Munich, Munich 80799, Germany;* orcid.org/0000-0001-7103-7060; Email: christoph.westerhausen@uni-a.de

### Authors

**Manuel M. Sirch** − *Institute of Theoretical Medicine, Physiology, University of Augsburg, Augsburg 86159, Germany; Institute of Physics, University of Augsburg, Augsburg 86159, Germany*

**David Wörle** − *Institute of Theoretical Medicine, Physiology, University of Augsburg, Augsburg 86159, Germany*

**Marina G. Huber** − *Institute of Theoretical Medicine, Physiology, University of Augsburg, Augsburg 86159, Germany*

Complete contact information is available at: https://pubs.acs.org/10.1021/acsomega.4c10054


### Notes

The authors declare no competing financial interest.

## ACKNOWLEDGMENTS

C.W. would like to acknowledge support by the Center for NanoScience (CeNS) and funding by the DFG (INST 94/135 FUGG 507881424 and 508235635). Moreover, C.W. an M.S. would like to acknowledge funding for the project "Physical and functional interaction mechanisms at cell membranes and vessel walls" by the University of Augsburg. All authors thank Dr. Torsten Gloe and Prof. Dr. Rudolf Schubert for fruitful discussions and Martin Richtsteig for technical support.

## REFERENCES

(1) Moghaddam, B.; McNeil, S. E.; Zheng, Q.; Mohammed, A. R.; Perrie, Y. Exploring the Correlation Between Lipid Packaging in Lipoplexes and Their Transfection Efficacy. *Pharmaceutics* **2011**, *3* (4), 848−864.

(2) Sun, M.; Dang, U. J.; Yuan, Y.; Psaras, A. M.; Osipitan, O.; Brooks, T. A.; Lu, F.; Di Pasqua, A. J. Optimization of DOTAP/chol Cationic Lipid Nanoparticles for mRNA, pDNA, and Oligonucleotide Delivery. *AAPS PharmSciTech* **2022**, *23* (5), 135.
(3) Lu, B.; Lim, J. M.; Yu, B.; Song, S.; Neeli, P.; Sobhani, N.; K, P.; Bonam, S. R.; Kurapati, R.; Zheng, J.; Chai, D. The next-generation DNA vaccine platforms and delivery systems: advances, challenges and prospects. *Front. Immunol.* **2024**, *15*, 1332939.
(4) Yin, H.; Kanasty, R.; Eltoukhy, A.; Vegas, A.; Dorkin, J. R.; Anderson, D. G. Non-viral vectors for gene-based therapy. *Nat. Rev. Genet.* **2014**, *15* (8), 541−555.
(5) Gandek, T. B.; van der Koog, L.; Nagelkerke, A. A Comparison of Cellular Uptake Mechanisms, Delivery Efficacy, and Intracellular Fate between Liposomes and Extracellular Vesicles. *Adv. Healthcare Mater.* **2023**, *12* (25), 2300319.
(6) Fu, L.; Kim, H. N.; Sterling, J. D.; Baker, S. M.; Lord, M. S. The role of the cell surface glycocalyx in drug delivery to and through the endothelium. *Adv. Drug Delivery Rev.* **2022**, *184*, 114195.
(7) Glassman, P. M.; Myerson, J. W.; Ferguson, L. T.; Kiseleva, R. Y.; Shuvaev, V. V.; Brenner, J. S.; Muzykantov, V. R. Targeting drug delivery in the vascular system: Focus on endothelium. *Adv. Drug Delivery Rev.* **2020**, *157*, 96−117.
(8) Yamamoto, K., Kamiya, A., Ando, J. Shear Stress Rapidly Alters the Physical Properties of Vascular Endothelial Cell Membranes by Decreasing Their Lipid Order and Increasing Their Fluidity. In: Roa Romero, L., Ed., *XIII Mediterranean Conference on Medical and Biological Engineering and Computing 2013. IFMBE Proceedings*; Springer: Cham, 2014, Vol. *41*; pp 19−22..
(9) He, Z.; Zhang, W.; Mao, S.; Li, N.; Li, H.; Lin, J.-M. Shear Stress-Enhanced Internalization of Cell Membrane Proteins Indicated by a Hairpin-Type DNA Probe. *Anal. Chem.* **2018**, *90* (9), 5540−5545.
(10) Espina, J. A.; Cordeiro, M. H.; Milivojevic, M.; Pajić-Lijaković, I.; Barriga, E. H. Response of cells and tissues to shear stress. *J. Cell Sci.* **2023**, *136* (18), jcs260985.
(11) Reitsma, S.; Slaaf, D. W.; Vink, H.; van Zandvoort, M. A. M. J.; oude Egbrink, M. G. A. The endothelial glycocalyx: composition, functions, and visualization. *Pflug. Arch. Eur. J. Physiol.* **2007**, *454* (3), 345−359.
(12) Moore, K. H.; Murphy, H. A.; George, E. M. The glycocalyx: a central regulator of vascular function. *Am. J. Physiol.: Regul., Integr. Comp. Physiol.* **2021**, *320* (4), R508−R518.
(13) Foote, C. A.; Soares, R. N.; Ramirez-Perez, F. I.; Ghiarone, T.; Aroor, A.; Manrique-Acevedo, C.; Padilla, J.; Martinez-Lemus, L. A. Endothelial Glycocalyx. *Compr. Physiol.* **2022**, *12* (4), 3781−3811.
(14) Li, X.; Zeng, S.; Wan, J.; Yang, Z.; Wang, F. The role of anesthetic drug and technique in endothelial glycocalyx: A narrative review. *Medicine (Baltimore)* **2023**, *102* (28), No. e34265.
(15) Curry, F. E.; Adamson, R. H. Endothelial Glycocalyx: Permeability Barrier and Mechanosensor. *Ann. Biomed. Eng.* **2012**, *40* (4), 828−839.
(16) Wang, G.; Kostidis, S.; Tiemeier, G. L.; Sol, W. M. P. J.; de Vries, M. R.; Giera, M.; Carmeliet, P.; van den Berg, B. M.; Rabelink, T. J. Shear Stress Regulation of Endothelial Glycocalyx Structure Is Determined by Glucobiosynthesis. *Arterioscler., Thromb., Vasc. Biol.* **2020**, *40* (2), 350−364.
(17) Becker, B. F.; Jacob, M.; Leipert, S.; Salmon, A. H. J.; Chappell, D. Degradation of the endothelial glycocalyx in clinical settings: searching for the sheddases. *Br. J. Clin. Pharmacol.* **2015**, *80* (3), 389−402.
(18) Mensah, S. A.; Nersesyan, A. A.; Harding, I. C.; Lee, C. I.; Tan, X.; Banerjee, S.; Niedre, M.; Torchilin, V. P.; Ebong, E. E. Flow-regulated endothelial glycocalyx determines metastatic cancer cell activity. *FASEB J.* **2020**, *34* (5), 6166−6184.
(19) Haymet, A. B.; Bartnikowski, N.; Wood, E. S.; Vallely, M. P.; McBride, A.; Yacoub, S.; Biering, S. B.; Harris, E.; Suen, J. Y.; Fraser, J. F. Studying the Endothelial Glycocalyx in vitro: What Is Missing? *Front. Cardiovasc. Med.* **2021**, *8*, 647086.
(20) Yamamoto, K.; Ando, J. Vascular endothelial cell membranes differentiate between stretch and shear stress through transitions in their lipid phases. *Am. J. Physiol. Regul. Integr. Comp.* **2015**, *309* (7), H1178−H1185.
(21) Butler, P. J.; Norwich, G.; Weinbaum, S.; Chien, S. Shear stress induces a time- and position-dependent increase in endothelial cell membrane fluidity. *Am. J. Physiol. Cell Physiol.* **2001**, *280* (4), C962−C969.
(22) Hirata, T.; Yamamoto, K.; Ikeda, K.; Arita, M. Functional lipidomics of vascular endothelial cells in response to laminar shear stress. *FASEB J.* **2021**, *35* (2), No. e2144.
(23) Zhang, F.; Lee, G. M.; Jacobson, K. Protein lateral mobility as a reflection of membrane microstructure. *BioEssays* **1993**, *15* (9), 579−588.
(24) Liu, J.; Sun, Y.; Drubin, D. G.; Oster, G. F. The Mechanochemistry of Endocytosis. *PLOS Biology* **2009**, *7* (9), No. e1000204.
(25) Sardar, A.; Dewangan, N.; Panda, B.; et al. Lipid and Lipidation in Membrane Fusion. *J. Membr. Biol.* **2022**, *255*, 691−703.
(26) Pachitariu, M.; Stringer, C. Cellpose 2.0: how to train your own model. *Nat. Methods* **2022**, *19*, 1634−1641.
(27) Morini, M. A.; Sierra, M. B.; Pedroni, V. I.; Alarcon, L. M.; Appignanesi, G. A.; Disalvo, E. A. Influence of temperature, anions and size distribution on the zeta potential of DMPC, DPPC and DMPE lipid vesicles. *Colloids Surf., B* **2015**, *131*, 54−58.
(28) Simberg, D.; Weisman, S.; Talmon, Y.; Barenholz, Y. DOTAP: Chemistry, biophysics, and transfection. *Crit. Rev. Ther. Drug Carrier Syst.* **2004**, *21* (4), 257−317.
(29) Stamatatos, L.; Leventis, R.; Zuckermann, M. J.; Silvius, J. R. Interactions of cationic lipid vesicles with negatively charged phospholipid vesicles and biological membranes. *Biochemistry* **1988**, *27* (11), 3917−3925.
(30) Böhringer, M.; Murugaiyan, J.; Eravci, M.; Weise, C.; Roesler, U.; Neubauer, H.; Sprague, L. D. Treatment of Yersinia similis with the cationic lipid DOTAP enhances adhesion to and invasion into intestinal epithelial cells - A proof-of-principle study. *Biochem. Biophys. Res. Commun.* **2020**, *524* (2), 373−379.
(31) Tarbell, J. M.; Ebong, E. E. The endothelial glycocalyx: a mechano-sensor and -transducer. *Sci. Signal.* **2008**, *1* (40), pt8.
(32) Ebong, E. E.; Macaluso, F. P.; Spray, D. C.; Tarbell, J. M. Imaging the endothelial glycocalyx in vitro by rapid freezing/freeze substitution transmission electron microscopy. *Arterioscler., Thromb., Vasc. Biol.* **2011**, *31* (8), 1908−1915.
(33) Serge, A. The Molecular Architecture of Cell Adhesion: Dynamic Remodeling Revealed by Videonanoscopy. *Front. Cell Dev. Biol.* **2016**, *4*, 36.
(34) Xu, G.-K.; Qian, J.; Hu, J. The glycocalyx promotes cooperative binding and clustering of adhesion receptors. *Soft Matter* **2016**, *12* (20), 4572−4583.
(35) Milusev, A.; Rieben, R.; Sorvillo, N. The Endothelial Glycocalyx: A Possible Therapeutic Target in Cardiovascular Disorders. *Front. Cardiovasc. Med.* **2022**, *9*, 897087.
(36) Möckl, L. The Emerging Role of the Mammalian Glycocalyx in Functional Membrane Organization and Immune System Regulation. *Front. Cell Dev. Biol.* **2020**, *8*, 253.
(37) Codini, M.; Garcia-Gil, M.; Albi, E. Cholesterol and Sphingolipid Enriched Lipid Rafts as Therapeutic Targets in Cancer. *Int. J. Mol. Sci.* **2021**, *22* (2), 726.
(38) Carotenuto, A. R.; Lunghi, L.; Piccolo, V.; Babaei, M.; Dayal, K.; Pugno, N.; Zingales, M.; Deseri, L.; Fraldi, M. Mechanobiology predicts raft formations triggered by ligand-receptor activity across the cell membrane. *J. Mech. Phys. Solids* **2020**, *141*, 103974.
(39) Vasantharajan, S. S.; Barnett, E.; Gray, E. S.; Rodger, E. J.; Eccles, M. R.; Pattison, S.; Munro, F.; Chatterjee, A. Size-Based Method for Enrichment of Circulating Tumor Cells from Blood of Colorectal Cancer Patients. *Methods Mol. Biol.* **2023**, *2588*, 231.


https://doi.org/10.1021/acsomega.4c10054
*ACS Omega* 2025, 10, 14858−14865